Directional Bloch surface wave coupling enabled by magnetic spin-momentum locking of light

Kaiwen Luo[1], Zhijing Huang[1], Xianpeng Lv[1], Wentao Qiu[1], Heyuan Guan[1], Tiefeng Yang[1], Thierry Grosjean[2**], Huihui Lu[1*]

[1] *Guangdong Provincial Key Laboratory of Optical Fiber Sensing and Communications, Department of Optoelectronic Engineering, Jinan University, Guangzhou510632, China*
[2] *CNRS, FEMTO-ST Institute UMR 6174, Université Bourgogne Franche-Comté, Besançon 25000, France*

ABSTRACT

We study the magnetic spin-locking of optical surface waves. Through an angular spectrum approach and numerical simulations, we predict that a spinning magnetic dipole develops a directional coupling of light to transverse electric (TE) polarized Bloch surface waves (BSWs). A high-index nanoparticle is placed on top of a one-dimensional photonic crystal to couple light into BSWs. Upon circularly polarized illumination, it mimics the spinning magnetic dipole. We find that the helicity of the light impinging on the nano-coupler controls the directionality of emerging BSWs. Further, identical silicon strip waveguides are configured on the two sides of the nano-coupler to confine and guide the BSWs. We achieve a directional nano-routing of the BSWs with circularly polarized illumination. Such a directional-coupling phenomenon has been proved to be solely mediated by the optical magnetic fields.

Address correspondence to Huihui Lu, thuihuilu@jnu.edu.cn; Thierry Grosjean, thierry.grosjean@univ-fcomte.fr

1 Introduction

Recent advances in nanophotonics have revealed the hidden role of magnetic field in light-matter interactions. Enhanced optical magnetic response can be obtained by using resonant metallic and dielectric nanostructures, which underpins a plethora of novel phenomena and applications such as negative refractive indices [1–4], controlling magnetic transitions [5–8], mapping optical magnetic field [9–14], etc. Besides, the magnetic component of light also contributes to the total spin density [15] and plays a significant role in optical spin-orbit interactions (SOI) [16, 17]. It has been shown that by means of SOI, remarkable magnetic effects can be achieved without optical resonances in nanostructures, which brings a new degree of freedom to light sensing and manipulation.

Our research refers to the spin-momentum locking of light — an optical SOI effect associated with evanescent waves. In such waves, the elliptically polarized electric or magnetic field describes a transverse spin angular momentum whose sign flips when propagating along opposite directions. With a subwavelength (dipolar) coupler, the longitudinal spin angular momentum (SAM) of an impinging wave can be transferred into the transverse SAM of the evanescent tail of a guided mode, leading to a directional light coupling and guiding wave. This robust spin-controlled directionality has been demonstrated with various optical systems including nanofiber [18], waveguide [19–22] and surface wave modes [23–27]. So far, most investigations focused on using the rotating electric component of light as the source of the SAM for originating the transverse spin-direction coupling [27–29]. A recent work demonstrated that the magnetic component of light can play the same role of offering SAM in the SOI of light [17]. In that work, the light coupler has an electric dipole response, leading to a power conversion to the Bloch surface waves (BSWs) driven by the electric optical field. The magnetic field is only responsible for the directionality control of the surface waves. Here, to exclude any influence from the electric field in the coupling process, we turn to use a magnetic dipole (MD) coupler and show a pure magnetic coupling of light to BSWs.

High-index dielectric nanoparticles can support MD mode. Working on Mie resonance, strong volume displacement currents are induced in these nanoparticles, which promotes the effective magnetic polarizability to be comparable or even stronger than the electric polarizability [30, 31]. High-index dielectric nanoparticles thus provide a versatile platform for studying magnetic light-matter interactions [30, 32–34]. Furthermore, the spectral position and relative strength of electric and magnetic optical resonances can also be independently tailored by changing the shape [35] and composite [36–38] of the nanoparticle. By this approach, a directional far-field scattering has been achieved. Besides, it has been revealed huge potential of high-index dielectric nanoantennas for directional excitation of surface waves and their highly efficient demultiplexing [35].

In this paper, we study the spin-locking of BSWs solely mediated by the magnetic field of light. BSWs are surface modes propagating on top of a one-dimensional photonic crystal (1D-PC) . We configure the dielectric multilayers of our 1D-PC to ensure a pure TE-polarized BSW mode in which only the magnetic field spins. A Mie scatterer is used as a near-field light-to-BSW coupler and circularly polarized light is projected onto the scatterer for studying the directional excitation of BSWs. We find that the excitation directionality of BSWs can be manipulated by spin-locking the magnetic SOI of light.

2 Angular spectrum representation of a dipole source

To start with, we consider a dipole source positioned just above a 1D-waveguide whose surface normal is parallel to **y**-axis. The

dipole moment is represented by $\boldsymbol{d}$ = [d_x, d_z], where d_x and d_z are the projections on the x- and z-axis, respectively. Such a model suffices to describe the scattering behavior of a Rayleigh particle [27], which herein lays the theoretical foundation for our study.

The dipole source is assumed located in air with a vertical distance $\boldsymbol{y_0}$ from the top surface of the waveguide. Its interaction with the waveguide can be described by Fermi's Golden Rule [39–42]. In general, this coupling scheme develops in the waveguide two guided modes that propagate toward the opposite ends. The directional excitation of the waveguide thus refers to the asymmetric distribution of the total coupled energy in the two counter-propagating guided waves. Such a coupling directionality originates from the interference of the respective optical excitations aroused by the two orthogonal components of the dipolar moment (d_x and d_z), which can be either destructive or constructive depending upon the propagation direction. Alternatively, this directional phenomenon can be interpreted from the dipole side by inspecting its angular spectrum [16, 43].

Following the angular momentum approach, a magnetic (electric) field can be resolved into a set of plane-wave and evanescent-wave components:

$$\mathbf{H}(x,y,z) = \iint \mathbf{H}(k_x,k_z)|_{y=y_0}\, e^{i(k_x x + k_z z + k_y |y-y_0|)} dk_x dk_z \qquad (1)$$

where $\mathbf{H}(x,y,z)$ and $\mathbf{H}(k_x,k_z)$ is the electromagnetic field represented in the real and the reciprocal spaces, respectively, k_x, k_y and k_z are the respective projections of the wavevector k along the x- , y-, and z-directions. We can also project the spatial component $\mathbf{H}(k_x,k_z)|_{y=y_0}$ with respect to the *s*- and *p*-polarizations of the electromagnetic field. Here, we are interested in a dipole moment rotating in the xz-plane, and hence consider only the unit vectors $\hat{e}_p$. We have:

$$\hat{e}_p(k_x,k_z) = \left(-\frac{k_x k_y}{k k_t}, -\frac{k_t}{k}\right), k_t = \sqrt{k_x^2 + k_z^2} \qquad (2)$$

where the – sign is taken since in our case the interesting spatial component is limited to the lower half-space (y < 0) .

To better understand the spin-locking effect while coupling a spinning dipole (elliptically or circularly polarized) to evanescent waves, we measure the dipolar directionality factor defined as follows:

$$\left[\frac{\hat{e}_p}{k_z}\right] \bullet d = \left(\frac{1}{k}\right)\left(-1, -\frac{k_x}{k_z}\right) \bullet (d_x, d_z) \qquad (3)$$

Figures 1(a) and 1(b) show the angular spectra of a dipole oriented in the z- and x-direction, respectively. While Figures 1(d) and 1(e) calculate the corresponding emission patterns of linear dipoles placed 10 nm above the glass/air interface. We can see that the angular spectrum is an odd function of k_x for the vertical dipole while even for the horizontal one. The superposition of the two dipoles can therefore lead to a strongly asymmetric function of k_x. By combining the two orthogonal dipoles with proper linear coefficients, the angular spectra of the dipoles with various polarization states are obtained and plotted in Figure 1(c). The composed dipolar field varies with the polarization state of the dipole. Remarkably, in certain cases, distinct symmetries appear in the propagating and evanescent spatial components.

As shown in Figure 1(c), the evanescent angular spectrum ($|k_x| > k$) of an elliptically or circularly polarized dipole is strongly asymmetric to k_x, which is in favor of a directionality in their near-field interaction with matters. The propagating components of these dipoles ($|k_x| < k$), however, are always symmetric disregarding the sign of k_x. Such a difference means that one can expect a directional phenomenon from a spinning dipole only by presenting it in proximity to the waveguide. In this way, the evanescent fields associated with the dipole and guided mode overlap and hence crosstalk efficiently. It is noted that, by introducing nanostructures to locally break the symmetry of an optical waveguide, directional phenomenon can also be realized with linear polarizations [44]. Nevertheless, when it comes to ordinary waveguides, one loses the directionality since a linear dipole contains symmetric evanescent components, as shown in Figure 1(c).

Quantitative assessment of the coupling directionality of a dipole to a waveguide can be made following the procedures described in literature [16, 27, 43]. According to that, the probability of exciting certain guided modes with specific (k_x, k_y) is proportional to the amplitude of the corresponding spatial component in the dipolar field, weighted by the Fresnel reflection coefficients [16]. Therefore, when a spinning dipole possessing a strongly asymmetric spectrum in its evanescent components is placed near to a surface or planar waveguide, it develops a highly directional excitation of the guided modes [16]. As can be inferred from Figure 1(c), a unidirectionality is attainable with proper helicity of the spinning magnetic dipole. Besides, one can play with the coupling directionality by tuning the ellipticity of the magnetic dipole. Such a tunable distribution of the coupled energy is ultimately due to the SAM transfer from the dipole source to the guided mode, which must obey the conservation law of angular momentum.

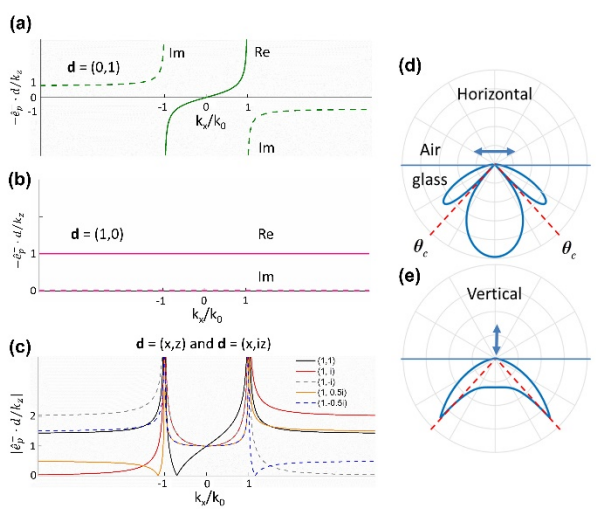

Figure 1. Angular spectrum presentation of dipoles with various

orientations and helicities. (a) A vertically-oriented linear dipole; (b) A horizontally-orientated linear dipole; (c) linear and rotating magnetic (electric) dipoles with various helicities. (d, e) Emission patterns of linear dipoles (vertical dipole and horizontal dipole) placed 10 nm above the glass/air interface.

So far, we have analytically shown that a spinning magnetic dipole could develop a spin-controlled excitation of optical guided modes. To verify that, we numerically investigate the coupling of circularly polarized magnetic and electric dipoles to BSWs by Finite-Difference Time-Domain (FDTD) method with a commercial code (Lumerical FDTD Solutions). To this end, we carry out two sets of simulations with the dipole positioned 10 nm above the top surface of a 1D-PC. The material and geometry of the 1D-PC is configured as those in previous literature [17] so that it supports a pure TE mode at the wavelength of 1550 nm.

Figure 2 shows the simulation results obtained by using electric and magnetic dipoles of various polarization states to excite the 1D-PC. We can see from Figures 2 (c-f) that the BSWs excited by a spinning magnetic dipole is strongly unbalanced on the left and right sides. The preferential side is dictated by the handedness of the dipole. It is noted that, however, a spinning electric dipole polarized in the xz-plane can hardly excite the TE-BSWs. A linearly polarized electric dipole oriented in the y-direction can excite the BSWs but leads to a symmetric distribution on both sides. A tunable directional excitation of the BSWs here is thus solely controlled by the magnetic field of light. Indeed, for TE-polarized BSWs only the magnetic field spins and describes the transverse SAM involved in the spin-locking effects [17].

From the above calculations, the directionality predicted by the angular momentum and numerical simulations matches well. Both show a tunable directionality controlled by the optical magnetic field.

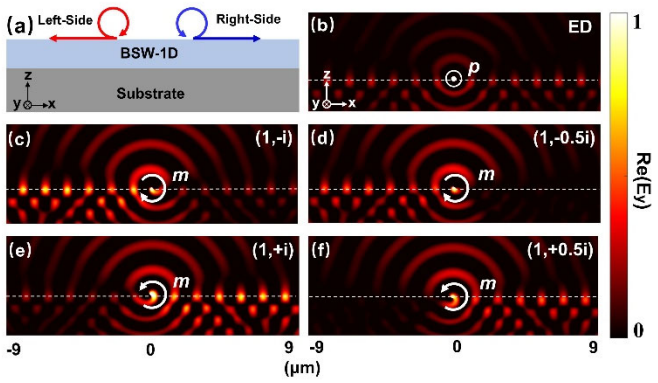

Figure 2. Coupling of circularly polarized magnetic and electric dipoles to BSWs. (a) Model of dipoles coupling to BSWs. (b) Y-component of electric field under the illumination of electric dipole source. (c-f) Y-components of electric field under the illumination of magnetic dipole sources (1, -i), (1, -0.5i), (1, i), (1, 0.5i), respectively.

3 Magnetic Resonances in Nanoparticles

A way to reach a spinning optical magnetic dipole consists of illuminating a dielectric nanosphere with an elliptically polarized light. Dielectric nanospheres of high-index (Si, Ge) material are known to support magnetic resonances described by a magnetic moment [32, 45]. Being spatially isotropic, such nanoparticles placed in a homogeneous environment can produce a spinning magnetic dipole of constant amplitude upon illumination with a circularly polarized light.

In this paper, we seek a spinning magnetic dipole at the wavelength of 1550 nm. To this end, two types of nanoparticles are investigated: i) a solid silicon sphere and ii) a core-shell structure with gold and silicon as the materials of the core and shell, respectively. We numerically study the dependence of scattering resonances on the sizes of these nanoparticles.

Figure 3(a) shows the scattering spectra of core-shell structures with a constant core radius of 70 nm and various shell radii ranging from 180 nm to 280 nm. As comparison, Figure 3(c) displays the scattering spectra of a silicon sphere whose radius is tailored within the same range. The scattering spectra of the two types of nanoparticles share some common characteristics. First, one can recognize three sources of optical resonance: the electric dipole (ED), magnetic dipole (MD) and magnetic quadrupole (MQ) resonances. The relative strength of these resonances varies with the structure size and operation wavelength. Second, the MQ resonance becomes much less significant around the wavelength of 1550 nm though it is remarkable at shorter wavelengths. Finally, in both structures the MD resonance dominates at $\lambda = 1550$ nm but in different reasons. As to the core-shell structure, this phenomenon results from the spectral overlapping of the ED and MD resonances as the radius of the silicon shell increases. For the silicon sphere, however, only the MD resonance holds at the wavelength around 1600 nm. These differences are more clearly shown in Figures 3(b) and 3(d), which plot the spectra of scattering cross-section of the MD and ED resonances, respectively.

From above discussion, one can see that both the silicon sphere and gold-silicon core-shell structure are good candidates for our purpose. However, it is known that the scattering and resonant properties of a dipolar source will be modified by a substrate presented nearby [46–48]. We numerically investigate the influences of the substrate on the optical responses of the nanoparticles. Figures 3(e) and 3(f) show respectively the simulated scattering cross-section spectra of the two nanoparticles in air and with two types of substrates presented, namely a dielectric slab and the 1D-PC. As shown in Figure 3(e), the dielectric slab redshifts the MD resonant peak of core-shell structure to 1600 nm while the 1D-PC only causes negligible spectral shift. A distinct influence of the substrate is found with the silicon sphere that both the dielectric slab and 1D-PC blue-shift the MD resonance by a comparable amount of 50 nm (see Figure 3(f)).

To clearly demonstrate the quantitative relationship between the electric and magnetic responses in nanoparticles, we give the formula to calculate the ratio of the MD components:

$$R = \frac{A_{MD}}{A_{ED} + A_{MD}} \times 100\% \qquad (4)$$

where A_{MD} and A_{ED} represent the amplitudes of the MD and ED at the peak of the scattering spectra around the wavelength of 1550 nm.

On resonance at $\lambda = 1550$ nm, the silicon sphere shows better MD response (R=83.1%) than the core-shell structure (R=76.2%). The MD-like optical response of the nanoparticles has been further confirmed by inspecting their emission

patterns. In these numerical studies, we use a commercial finite-element electromagnetic solver (the RF module of COMSOL Multiphysics). The results are shown in Figures 3(g), 3(h) and Figure S1 of Electronic Supplementary Material. Such a doughnut shape characterizes the far-field of an MD which is shown in Figure (h). Indeed, if considerable amount of ED or high-order multipole resonances were involved, the scattering pattern would lose its perfect symmetry [49]. Therefore, with the optimal design of the two nanoparticles, we have found that the silicon sphere with a radius of 220nm exhibits better MD properties than the core-shell structure at $\lambda = 1550\,\mathrm{nm}$ with the presence of the 1D-PC.

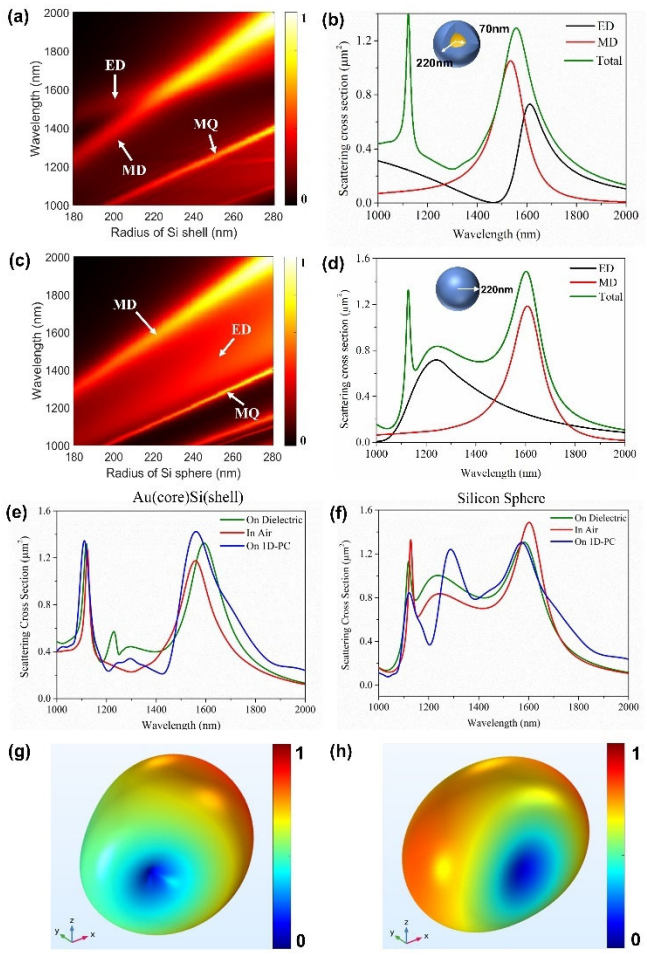

Figure 3. (a) The evolution of Mie resonances of a gold core of 140nm in diameter with increasing radius of silicon shell. (b) The decomposition of scattering spectrum for the Au core/silicon shell nanoparticle. The outer radius R of silicon shell is 220 nm. (c) The evolution of Mie resonances of a silicon sphere with the increase of radius. (d) The decomposition of scattering spectrum for the silicon sphere with the radius of 220 nm. (e, f) Substrate modified scattering behavior of nanoparticles for Au (core) Si (shell) and Silicon nanosphere. (g, h) The far-field scattering pattern of the Au (core) Si (shell) nanoparticle and silicon sphere in the air at the MD resonance wavelength of 1550 nm, respectively.

4 Directionality control of BSWs from a Si nano sphere on a 1D-PC

By using a near-field coupler, one can couple the optical energy from propagating light to Bloch surface waves. Such couplers can be an individual air groove [17] milled in the top layer of the waveguide structure or a nanoparticle positioned just above [50]. Figure S2 of Electronic Supplementary Material show the symmetric electric field excited by the nanoparticle under the illumination of circularly polarized Gaussian beam at normal incidence, which indicates that the BSWs excited in this case are not directional. In order to observe the spin-locking effect, one need to illuminate these dipole-like couplers with elliptically polarized light at glancing angle so that the spinning dipole moment can be excited. In this way, the SAM carried by the free-space photons can be transferred to the transverse SAM of the surface waves during the energy coupling process [17].

The above-described scheme has been used to demonstrate the spin-locking effects associated with the electric or magnetic fields of light [17]. We follow this idea and adopt a silicon sphere as the light-to-BSW coupler (see Figure 4(a)). It is noted that, the nanoparticle merely produces a symmetric field distribution under the illumination of linear polarized incident light, as shown in Figure 4(b).

We illuminate the nanoparticles at four oblique angles (α =30°, 45°, 60°, and 80°) to see how the spin-locking effect comes to work. Figure 4(c) shows the corresponding simulation results obtained with circular polarized light of opposite handedness. The elongated spot indicated by the thicker white arrow is the cross-section of the excitation beam along the surface the 1D-PC. The two thinner white arrows mark the emerging BSWs where one can see an unbalanced intensity distribution on the two sides. Besides, the preferential excitation toggles from one side to the other as we inverse the handedness of the incident light, revealing a spin-dependent characteristic of this phenomenon. As the incident angle increases, the intensity distribution asymmetry in the emerging BSWs becomes more and more pronounced. When α =80°, the coupled energy is almost steered to only one side. Such a directional BSW excitation is also visible in the far-field scattering patterns shown in Figure 4(d). Moreover, Figures 4(e) and 4(f) show that under the illumination of circularly polarized incident light at the angle of 80°, the BSWs on the side of stronger intensity are off-center by about 30 degrees.

We see above that the coupling directionality improves as the incident angle increases. That is because the SAM of the BSWs is transverse while that of the incident photons is longitudinal regarding their respective propagation directions. A larger incident angle of the impinging light will lead to a better alignment of the two SAMs and thus a higher coupling directionality. In purely TE-polarized BSWs only the magnetic field rotates. Therefore, the observed spin-locking directionality is solely controlled by the magnetic fields of the incident light.

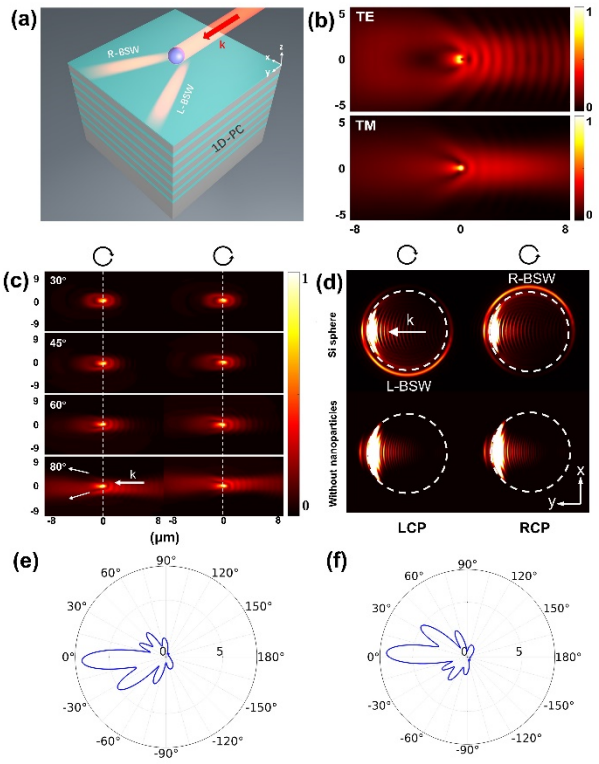

Figure 4. (a) Model of a silicon sphere on 1D-PC illuminated by different polarizations of light. (b) Symmetric electric field distribution under the illumination of linear polarized incident light at the angle of 80° (TE and TM polarization). (c) Electric field distributions under different incident angle of circular polarized light. (d) The far field radiation image under different polarization states of incident light with titled angle of 80°. (e, f) Far-field scattering patterns of the silicon sphere on the 1D-PC under the illumination of left-circularly polarized and right-circularly polarized incident light at the angle of 80°, respectively.

5 The energy coupling to BSWs

We also numerically study the directional excitation of BSWs in a more realistic optical setup suggested in Ref. [17]: light passes through a fixed linear polarizer (LP) and a rotating quarter-wave plate (QWP) inserted successively and impinges on the nanoparticle at a glancing angle ($\alpha = 80°$). Assigning θ as the rotation angle of the QWP measured from its fast axis to the transmission axis of the LP (x-axis), the output polarization state can be described using Jones matrix calculus:

$$\boldsymbol{J}'(\theta) = \boldsymbol{R}^{-1}(\theta) \times \boldsymbol{M} \times \boldsymbol{R}(\theta) \times \boldsymbol{J} \qquad (5)$$

Here, $\boldsymbol{J}$ and $\boldsymbol{J}'$ are the Jones vectors of light just after the LP and the QWP, respectively. $\boldsymbol{R}^{-1}(\theta) \times \boldsymbol{M} \times \boldsymbol{R}(\theta)$ represents the polarization transformation function of the QWP: $\boldsymbol{M}$ defines the phase retardation introduced to the fast and slow axes while $\boldsymbol{R}^{-1}(\theta)$ and $\boldsymbol{R}(\theta)$ account for the rotation effect. In our case, $\boldsymbol{J}'$ generally defines a rotating polarization ellipse whose orientation and ellipticity changes with a single parameter θ. More specifically, the output polarization state is circular and linear when $\theta = 45° + k90°$ (k = 0, 1, 2, 3) and $\theta = k90°$ (k = 0, 1, 2, 3), respectively. It is elliptical for intermediate angles.

The rotation of QWP regarding the fixed LP dynamically modulates the properties of the light impinging on the nanoparticle. Its helicity has a 180°-periodicity with respect to the angle θ, which thus dictates a 2θ-dependence for any helicity-dependent optical phenomena. Besides, the electromagnetic amplitude of the incident light, when projected on the polarization vectors of BSWs, also undergoes a 2θ-modulation. Therefore, the excitation rate of BSWs has a 4θ-dependence due to their proportionality to the optical intensity. Such modulations of different periodicity are critical for identifying the origins the magnetic spin-locking effect [17]. In our numerical simulations (FDTD method), two lights of orthogonal linear polarizations are used separately to excite the nanoparticle. The obtained results are linearly combined to construct the result at an arbitrary polarization state of the incident light. The combination coefficients are identical to the elements in $\boldsymbol{J}'$. We consider a 360°-rotation of the QWP and plot the intensity of BSWs on the left and right sides as a function of θ. The integral area of the electric field is shown in Figure S3(a) of Electronic Supplementary Material. We can see that in Figure 5 all BSW intensity curves show similar characteristics, namely a 4θ-harmonic function undergoing a 2θ-harmonic modulation. Besides, one can see from the curves a spin-dependent directionality with a 180°-periodicity. These observations are consistent with our predictions.

To better understand the 2θ- and 4θ-modulations in the recorded signals, we apply Fourier transforms to get them expressed in the following analytical form:

$$S_j(\theta) = A_j^{(0)} + A_j^{(2)} \sin\left(2\theta + \phi_j^{(2)}\right) + A_j^{(4)} \sin\left(4\theta + \phi_j^{(4)}\right) \qquad (6)$$

Here, the subscription *j=R, L* indicates the right- and left-side, respectively. The superscription denotes the order of the harmonic components whose amplitude and phase are A_j and ϕ_j, respectively.

As shown in Figure 5, the intensity signals consist of harmonic functions of the zeroth, second and fourth order. The second harmonics is associated with the energy coupling from light into BSWs resulting from the spin-controlled distribution. Moreover, due to the TE-polarized nature of our BSWs (only the magnetic field spins), such a helicity-dependent energy distribution is solely related to the magnetic field of the incident light. It is noted that, since here we use a MD coupler, both the second and fourth harmonics should be attributed to magnetic effects. This is different from Ref. 17 where an electric coupler was used (see Table S1 of Electronic Supplementary Material).

We see that in Figure 5(b) the ratio of the second harmonic component to the fourth harmonic is higher than that in Figure 5(d), which shows that magnetic optical effect plays a larger role in spin-controlled coupling by using a silicon sphere. (For more details, please refer to Figure S3 (b) of Electronic Supplementary Material).

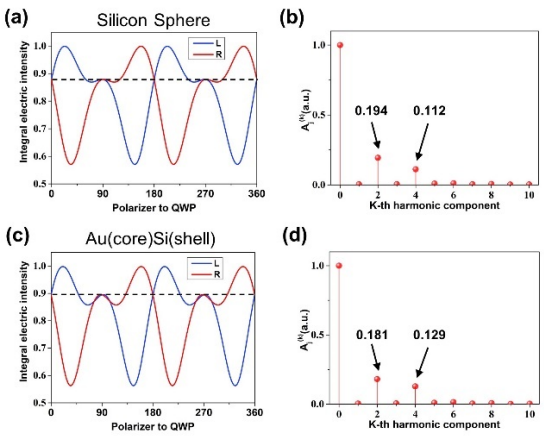

Figure 5. (a, c) Electric intensity of the dipole-excited Bloch surface waves for different incident polarization states from silicon nanosphere and Au core/silicon shell. (b, d) Fourier analysis of right-side and left-side signal of silicon nanosphere and Au core/silicon shell, respectively.

6 Waveguide coupling

Figure 6(a) shows another photonic platform we use for demonstrating the directional excitation of BSWs mediated by the magnetic SOI of light. The 1D-PC and the light coupler (silicon nanosphere, radius: 0.22-μm) are identical to the ones described in Sec. **4**. We shed light on the nanoparticle at an incident angle of 80°. As shown previously, BSWs will be excited on both sides of the nanoparticle. To better pick up the BSW signals from the spurious background of the incoming light beam, we place silicon strip waveguides along the trajectories of BSWs. The silicon waveguides are 10-μm long and have a square cross-section with a side length of 0.44 μm. The center of the silicon waveguides is 7.26μm away from the center of the nanoparticle, and the angle between the waveguides is set to 60°. As shown in Figure 6(a), the BSW signal is coupled to a guide mode in the silicon waveguide.

Given the symmetry of our photonic platform, the optical energies transmitted in the two silicon waveguides are proportional to those coupled from the incident light to the left and right branches of BSWs. The excitation directionality of BSWs can thus be evaluated with the following directionality factor:

$$C = \frac{\int |E_R|^2 \, dS}{\int |E_L|^2 \, dS} \tag{7}$$

where $E = \sqrt{|E_X|^2 + |E_Y|^2 + |E_Z|^2}$ and the integral is taken over the cross section of the silicon waveguide on the left and right sides, as represented by the subscript "L" and "R" in Figure 6(a), respectively.

Figures 6(b) and 6(c) show the propagating modes excited in the silicon waveguides upon circularly polarized illumination of opposite handedness. They show a strongly unbalanced intensity distribution in the two waveguides with a directionality factor $\boldsymbol{C}$ up to 4.58 in Figure 6(b). Besides, inversing the handedness of the incident light switches the prevailing side from one to another with a directionality factor $\boldsymbol{C}$ = 1/4.58, manifesting a spin-dependent characteristic of this phenomenon. As a contrast, with linearly polarized incident light, the coupled energy is equally distributed ($\boldsymbol{C}$ = 1). According to Sec. **5**, changing the polarization state of the incident light allows us to tunably control the value of $\boldsymbol{C}$, which can be utilized to build on-chip light routers.

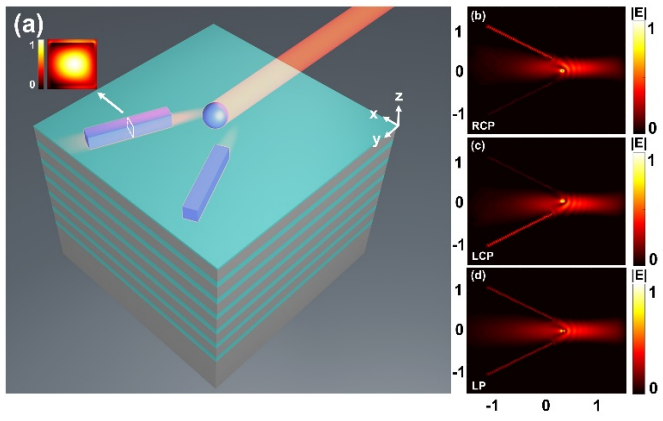

Figure 6. (a) 1D-PC model and the guide mode of the silicon waveguide. (b,c) The field distribution of the structure under the illumination of circular incident light after two silicon waveguides are placed on the propagation track (The source of **b** is RCP and **c** is LCP). (d) The field distribution of the structure under the illumination of linearly polarized light.

7 Conclusions

We present a new demonstration of the magnetic spin-orbit interaction (SOI) of light. We show that a circularly polarized MD source develops a tunable unidirectional coupling of light into TE-polarized BSWs: depending on the helicity of the MD, the optical surface waves was preferentially excited on the left or right side. The underlying physics is the coupling between the longitudinal SAM of the freely propagating photons and the transverse SAM in the evanescent tails of the guided BSWs. The SAM involved in the coupling process is solely described by the rotating magnetic field of light. We further use MD-like nanoparticles as the light-to-BSW converter and silicon stripe waveguides to collect the emerging BSWs. Upon circularly polarized illumination, the ratio of the optical intensities in the left and right waveguides reach a value up to 4.58. In our study, the magnetic field is not only responsible for the transfer of energy to the BSW, but also controls the directionality of the coupled energy. We thus demonstrate a tunable spin-locking phenomenon characteristic of a pure magnetic effect.

Acknowledgements

This research was funded in part by the National Natural Science Foundation of China (61775084, 62075088), the NSAF (U2030103), the Natural Science Foundation of Guangdong Province (2020A1515010791, 2021A0505030036), the Open Fund of Guangdong Provincial Key Laboratory of Information Photonics Technology of Guangdong University of Technology (GKPT20-03) and the Fundamental Research Funds for the Central Universities (21622107, 21622403), we acknowledge Dr. Mengjia Wang for his helpful discussion.

Electronic Supplementary Material: Supplementary material (the far-field scattering pattern of the silicon sphere in the air at the wavelength of 1600nm (Figure S1); the electric field excited by the nanoparticle and the electric field on the surface of the 1D-PC without nanoparticle under the illumination of circularly polarized Gaussian beam at normal incidence (Figure S2); the area where the electric field is integrated and ratio (the second harmonic component/ the fourth harmonic component) of

different nanoparticles (Figure S3)) is available in the online version of this article at http://dx.doi.org/10.1007/s12274-***-****-* (automatically inserted by the publisher).

References

[1] Zhang, S.; Jiang, R.; Xie, Y. M.; Ruan, Q.; Yang, B.; Wang, J.; Lin, H. Q. Colloidal Moderate-Refractive-Index Cu2O Nanospheres as Visible-Region Nanoantennas with Electromagnetic Resonance and Directional Light-Scattering Properties. Adv. Mater. **2015**, 27, 7432–7439.

[2] Paniagua-Domínguez, R.; López-Tejeira, F.; Marqués, R.; Sánchez-Gil, J. A. Metallo-Dielectric Core-Shell Nanospheres as Building Blocks for Optical Three-Dimensional Isotropic Negative-Index Metamaterials. New J. Phys. **2011**, 13, 123017.

[3] Smith, D. R.; Pendry, J. B.; Wiltshire, M. C. K. Metamaterials and Negative Refractive Index. Science. **2004**, 305, 788–792.

[4] Shalaev, V. M. Optical Negative-Index Metamaterials. Nat. Photonics **2007**, 1, 41–48.

[5] Taminiau, T. H.; Karaveli, S.; Van Hulst, N. F.; Zia, R. Quantifying the Magnetic Nature of Light Emission. Nat. Commun. **2012**, 3, 976–979.

[6] Rolly, B.; Bebey, B.; Bidault, S.; Stout, B.; Bonod, N. Promoting Magnetic Dipolar Transition in Trivalent Lanthanide Ions with Lossless Mie Resonances. Phys. Rev. B. **2012**, 85, 245432.

[7] Hein, S. M.; Giessen, H. Tailoring Magnetic Dipole Emission with Plasmonic Split-Ring Resonators. Phys. Rev. Lett. **2013**, 111, 026803.

[8] Mivelle, M.; Grosjean, T.; Burr, G. W.; Fischer, U. C.; Garcia-Parajo, M. F. Strong Modification of Magnetic Dipole Emission through Diabolo Nanoantennas. ACS Photonics. **2015**, 2, 1071–1076.

[9] Devaux, E.; Dereux, A.; Bourillot, E.; Weeber, J. C.; Lacroute, Y.; Goudonnet, J. P. Local Detection of the Optical Magnetic Field in the near Zone of Dielectric Samples. Phys. Rev. B. **2000**, 62, 10504–10514.

[10] Le Feber, B.; Rotenberg, N.; Beggs, D. M.; Kuipers, L. Simultaneous Measurement of Nanoscale Electric and Magnetic Optical Fields. Nat. Photonics. **2014**, 8, 43–46.

[11] Kihm, H. W.; Koo, S. M.; Kim, Q. H.; Bao, K.; Kihm, J. E.; Bak, W. S.; Eah, S. H.; Lienau, C.; Kim, H.; Nordlander, P.; Halas, N. J.; Park, N. K.; Kim, D. S. Bethe-Hole Polarization Analyser for the Magnetic Vector of Light. Nat. Commun. **2011**, 2, 451.

[12] Grosjean, T.; Fahys, A.; Suarez, M.; Charraut, D.; Salut, R.; Courjon, D. Annular Nanoantenna on Fibre Micro-Axicon. J. Microsc. **2008**, 229, 354–364.

[13] Burresi, M.; Van Oosten, D.; Kampfrath, T.; Schoenmaker, H.; Heideman, R.; Leinse, A.; Kuipers, L. Probing the Magnetic Field of Light at Optical Frequencies. Science. **2009**, 326, 550–553.

[14] Suarez, M. A.; Grosjean, T.; Charraut, D.; Courjon, D. Nanoring as a Magnetic or Electric Field Sensitive Nano-Antenna for near-Field Optics Applications. Opt. Commun. **2007**, 270, 447–454.

[15] Neugebauer, M.; Bauer, T.; Aiello, A.; Banzer, P. Measuring the Transverse Spin Density of Light. Phys. Rev. Lett. **2015**, 114, 063901.

[16] Picardi, M. F.; Manjavacas, A.; Zayats, A. V.; Rodríguez-Fortuño, F. J. Unidirectional Evanescent-Wave Coupling from Circularly Polarized Electric and Magnetic Dipoles: An Angular Spectrum Approach. Phys. Rev. B. **2017**, 95, 245416.

[17] Wang, M.; Zhang, H.; Kovalevich, T.; Salut, R.; Kim, M. S.; Suarez, M. A.; Bernal, M. P.; Herzig, H. P.; Lu, H.; Grosjean, T. Magnetic Spin-Orbit Interaction of Light. Light Sci. Appl. **2018**, 7, 24.

[18] Petersen, J.; Volz, J.; Rauschenbeutel, A. Chiral Nanophotonic Waveguide Interface Based on Spin-Orbit Interaction of Light. Science. **2014**, 346, 67–71.

[19] Rodríguez-Fortuño, F. J.; Barber-Sanz, I.; Puerto, D.; Griol, A.; Martínez, A. Resolving Light Handedness with an On-Chip Silicon Microdisk. ACS Photonics. **2014**, 1, 762–767.

[20] Lefier, Y.; Grosjean, T. Unidirectional Sub-Diffraction Waveguiding Based on Optical Spin–Orbit Coupling in Subwavelength Plasmonic Waveguides. Opt. Lett. **2015**, 40, 2890.

[21] Le Feber, B.; Rotenberg, N.; Kuipers, L. Nanophotonic Control of Circular Dipole Emission. Nat. Commun. **2015**, 6, 6695.

[22] Lefier, Y.; Salut, R.; Suarez, M. A.; Grosjean, T. Directing Nanoscale Optical Flows by Coupling Photon Spin to Plasmon Extrinsic Angular Momentum. Nano Lett. **2018**, 18, 38–42.

[23] Lee, S. Y.; Lee, I. M.; Park, J.; Oh, S.; Lee, W.; Kim, K. Y.; Lee, B. Role of Magnetic Induction Currents in Nanoslit Excitation of Surface Plasmon Polaritons. Phys. Rev. Lett. **2012**, 108, 213907.

[24] Mueller, J. P. B.; Leosson, K.; Capasso, F. Polarization-Selective Coupling to Long-Range Surface Plasmon Polariton Waveguides. Nano Lett. **2014**, 14, 5524–5527.

[25] Xi, Z.; Lu, Y.; Yu, W.; Wang, P.; Ming, H. Unidirectional Surface Plasmon Launcher: Rotating Dipole Mimicked by Optical Antennas. J. Opt. **2014**, 16, 105002.

[26] Lin, J.; Mueller, J. P. B.; Wang, Q.; Yuan, G.; Antoniou, N.; Yuan, X. C.; Capasso, F. Polarization-Controlled Tunable Directional Coupling of Surface Plasmon Polaritons. Science. **2013**, 340, 331–334.

[27] Rodríguez-fortuño, F. J.; Martínez, A.; Wurtz, G. a; Zayats, A. V. Near-Field Interference for the Unidirectional Excitation of Electromagnetic Guided Modes. Science. **2013**, 340, 328–330.

[28] Bliokh, K. Y.; Nori, F. Transverse Spin of a Surface Polariton. Phys. Rev. A. **2012**, 85, 061801.

[29] Kim, K. Y.; Lee, I. M.; Kim, J.; Jung, J.; Lee, B. Time Reversal and the Spin Angular Momentum of Transverse-Electric and Transverse-Magnetic Surface Modes. Phys. Rev. A. **2012**, 86, 063805.

[30] Kuznetsov, A. I.; Miroshnichenko, A. E.; Brongersma, M. L.; Kivshar, Y. S.; Luk'yanchuk, B. Optically Resonant Dielectric Nanostructures. Science. **2016**, 354, 2472.

[31] Colom, R.; Devilez, A.; Enoch, S.; Stout, B.; Bonod, N. Polarizability Expressions for Predicting Resonances in Plasmonic and Mie Scatterers. Phys. Rev. A. **2017**, 95, 063833.

[32] García-Etxarri, A.; Gómez-Medina, R.; Froufe-Pérez, L. S.; López, C.; Chantada, L.; Scheffold, F.; Aizpurua, J.; Nieto-Vesperinas, M.; Sáenz, J. J. Strong Magnetic Response of Submicron Silicon Particles in the Infrared. Opt. Express. **2011**, 19, 4815–4826.

[33] Kuznetsov, A. I.; Miroshnichenko, A. E.; Fu, Y. H.; Zhang, J.; Luk, B. Magnetic Light. Sci. Rep. **2012**, 2, 492.

[34] Evlyukhin, A. B.; Novikov, S. M.; Zywietz, U.; Eriksen, R. L.; Reinhardt, C.; Bozhevolnyi, S. I.; Chichkov, B. N. Demonstration of Magnetic Dipole Resonances of Dielectric Nanospheres in the Visible Region. Nano Lett. **2012**, 12, 3749–3755.

[35] Sinev, I. S.; Bogdanov, A. A.; Komissarenko, F. E.; Frizyuk, K. S.; Petrov, M. I.; Mukhin, I. S.; Makarov, S. V.; Samusev, A. K.; Lavrinenko, A. V.; Iorsh, I. V. Chirality Driven by Magnetic Dipole Response for Demultiplexing of Surface Waves. Laser Photonics Rev. **2017**, 11, 1700168.

[36] Wei Liu, Jianfa Zhang, Bing Lei, Haotong Ma, Wenke Xie, and H. H. Ultra-Directional Forward Scattering by Individual Core-Shell Nanoparticles. Opt. Express. **2014**, 22, 16178–16187.

[37] Liu, W.; Miroshnichenko, A. E.; Neshev, D. N.; Kivshar, Y. S. Broadband Unidirectional Scattering by Magneto-Electric Core-Shell Nanoparticles. ACS Nano. **2012**, 6, 5489–5497.

[38] Shen, F.; An, N.; Tao, Y.; Zhou, H.; Jiang, Z.; Guo, Z. Anomalous Forward Scattering of Gain-Assisted Dielectric Shell-Coated Metallic Core Spherical Particles. Nanophotonics. **2017**, 6, 1063–1072.

[39] Kingsley-Smith, J. J.; Picardi, M. F.; Wei, L.; Zayats, A. V.; Rodríguez-Fortuño, F. J. Optical Forces from Near-Field Directionalities in Planar Structures. Phys. Rev. B. **2019**, 99, 235410.

[40] Picardi, M. F.; Zayats, A. V.; Rodríguez-Fortuño, F. J. Janus and Huygens Dipoles: Near-Field Directionality beyond Spin-Momentum Locking. Phys. Rev. Lett. **2018**, 120, 117402.

[41] Jan Petersen, Jürgen Volz, A. R. Chiral Nanophotonic Waveguide Interface Based on Spin-Orbit Interaction of Light. Science. **2014**, 346, 67–71.

[42] Espinosa-Soria, A.; Martínez, A. Transverse Spin and Spin-Orbit Coupling in Silicon Waveguides. IEEE Photonics Technol. Lett. **2016**, 28, 1561–1564.

[43] F. Picardi, M.; V. Zayats, A.; J. Rodríguez-Fortuño, F. Amplitude and Phase Control of Guided Modes Excitation from a Single Dipole Source:

Engineering Far- and Near-Field Directionality. Laser Photonics Rev. **2019**, 13, 1900250.

[44] Rodríguez-Fortuño, F. J.; Puerto, D.; Griol, A.; Bellieres, L.; Martí, J.; Martínez, A. Sorting Linearly Polarized Photons with a Single Scatterer. Opt. Lett. **2014**, 39, 1394–1397.

[45] Gómez-Medina, R. Electric and Magnetic Dipolar Response of Germanium Nanospheres: Interference Effects, Scattering Anisotropy, and Optical Forces. J. Nanophotonics. **2011**, 5, 053512.

[46] van de Groep, J.; Polman, A. Designing Dielectric Resonators on Substrates: Combining Magnetic and Electric Resonances. Opt. Express. **2013**, 21, 26285–26302.

[47] Sinev, I.; Iorsh, I.; Bogdanov, A.; Permyakov, D.; Komissarenko, F.; Mukhin, I.; Samusev, A.; Valuckas, V.; Kuznetsov, A. I.; Luk'yanchuk, B. S.; Miroshnichenko, A. E.; Kivshar, Y. S. Polarization Control over Electric and Magnetic Dipole Resonances of Dielectric Nanoparticles on Metallic Films. Laser Photonics Rev. **2016**, 10, 799–806.

[48] Markovich, D. L.; Ginzburg, P.; Samusev, A. K.; Belov, P. A.; Zayats, A. V. Magnetic Dipole Radiation Tailored by Substrates: Numerical Investigation. Opt. Express. **2014**, 22, 10693–10702.

[49] Feng, T.; Xu, Y.; Zhang, W.; Miroshnichenko, A. E. Ideal Magnetic Dipole Scattering. Phys. Rev. Lett. **2017**, 118, 173901.

[50] Gulkin, D. N.; Popkova, A. A.; Afinogenov, B. I.; Shilkin, D. A.; Kuršelis, K.; Chichkov, B. N.; Bessonov, V. O.; Fedyanin, A. A. Mie-Driven Directional Nanocoupler for Bloch Surface Wave Photonic Platform. Nanophotonics. **2021**, 10, 2939–2947.

Electronic Supplementary Material

Magnetic spin-locking of light direct Bloch surface wave

Kaiwen Luo[1], Zhijing Huang[1], Xianpeng Lv[1], Wentao Qiu[1], Heyuan Guan[1], Thierry Grosjean[2](✉), Huihui Lu[1] (✉)

[1] *Guangdong Provincial Key Laboratory of Optical Fiber Sensing and Communications, Department of Optoelectronic Engineering, Jinan University, Guangzhou510632, China*
[2] *CNRS, FEMTO-ST Institute UMR 6174, Université Bourgogne Franche-Comté, Besançon 25000, France*

Supporting information to DOI 10.1007/s12274-****-****-* (automatically inserted by the publisher)

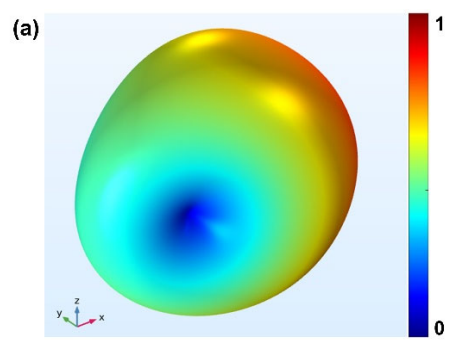

Figure S1 The far-field scattering pattern of the silicon sphere in the air at the wavelength of 1600nm.

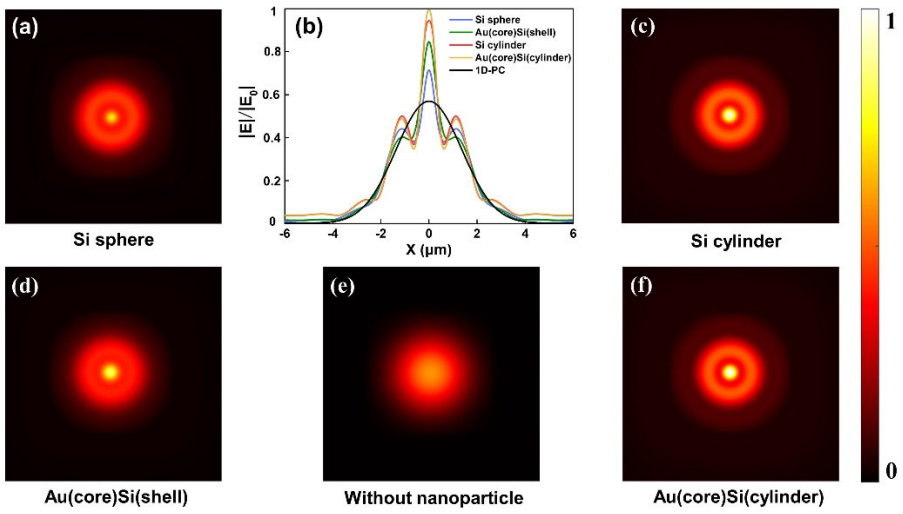

Figure S2 The electric field excited by the nanoparticle and the electric field on the surface of the 1D-PC without nanoparticle under the illumination of circularly polarized Gaussian beam at normal incidence.

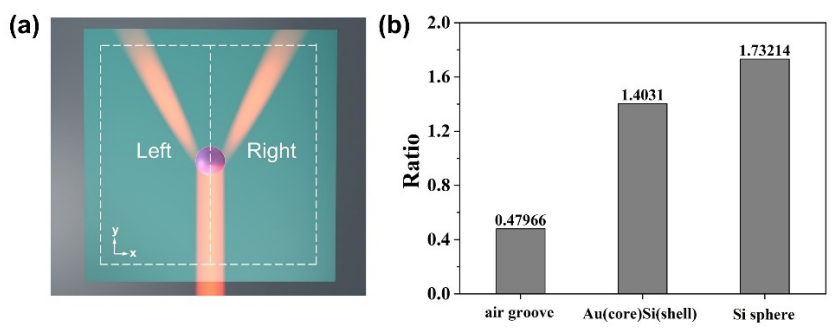

Address correspondence to Huihui Lu, thuihuilu@jnu.edu.cn; Thierry Grosjean, thierry.grosjean@univ-fcomte.fr

Figure S3 (a) The area where the electric field is integrated. Symmetrically divide the simulation region into two parts. And then we collected the electric intensity both right side and left side. (b) Ratio (the second harmonic component/ the fourth harmonic component) of different nanoparticles.

Table S1 Comparison between our work and literature [1].

	Light-to-BSW coupler	2nd harmonics	4th harmonics
Wang: lsa2018 [1]	Air groove (ED coupler)	Magnetic effect	Electric effect
This work	Mie particle (MD coupler)	Magnetic effect	Magnetic effect

References

[1] Wang, M.; Zhang, H.; Kovalevich, T.; Salut, R.; Kim, M. S.; Suarez, M. A.; Bernal, M. P.; Herzig, H. P.; Lu, H.; Grosjean, T. Magnetic Spin-Orbit Interaction of Light. Light Sci. Appl. 2018, 7, 24.